Understanding and controlling photothermal responses in MXenes

Burak Guzelturk^{1,#,*}, Vladislav Kamysbayev^{2,#}, Di Wang^{2,#}, Huicheng Hu², Ruiyu Li², Sarah B. King², Alexander H. Reid³, Ming-Fu Lin³, Xijie Wang³, Donald A. Walko¹, Xiaoyi Zhang¹, Aaron Lindenberg^{4,5}, Dmitri V. Talapin^{2,6*}

These authors contributed equally to this work

Correspondence to: burakg@anl.gov and dvtalapin@uchicago.edu

Abstract:

MXenes have the potential for efficient light-to-heat conversion in photothermal applications. To effectively utilize MXenes in such applications, it is important to understand the underlying nonequilibrium processes, including electron-phonon and phonon-phonon couplings. Here, we use transient electron and X-ray diffraction to investigate the heating and cooling of photoexcited MXenes at femtosecond to nanosecond timescales. Our results show extremely strong electron-phonon coupling in Ti₃C₂-based MXenes resulting in lattice heating within a few hundred femtoseconds. We also systematically study heat dissipation in MXenes with varying film thickness, chemical surface termination, flake size, and annealing conditions. We find that the thermal boundary conductance (TBC) governs the thermal relaxation in films thinner than the optical penetration depth. We achieve a two-fold enhancement of the TBC reaching 20 MW m⁻²

¹ X-ray Science Division, Argonne National Laboratory, Lemont, IL 60439, United States

² Department of Chemistry, James Franck Institute, and Pritzker School of Molecular Engineering, University of Chicago, Chicago, IL 60637, USA

³ SLAC National Accelerator Laboratory, Menlo Park, CA 94025, USA

⁴ Department of Materials Science and Engineering, Stanford University, Stanford, CA 94305, USA

⁵ Stanford Institute for Materials and Energy Sciences, SLAC National Accelerator Laboratory, Menlo Park, CA 94025, USA

⁶ Center for Nanoscale Materials, Argonne National Laboratory, Lemont, IL 60439, United States

K⁻¹ by controlling flake size or chemical surface termination, which is promising for engineering heat dissipation in photothermal and thermoelectric applications of the MXenes.

Keywords: MXenes, Ti₃C₂T_x, photothermal properties, ultrafast electron diffraction, time-resolved X-ray scattering

Two-dimensional transition metal carbides, carbonitrides and nitrides, known as MXenes¹, have attracted extensive research attention due to their remarkable electronic, optical, magnetic and chemical properties^{2–4}. These properties make them suitable in a wide range of applications, including transparent conductors⁵, electromagnetic shielding⁶, energy storage⁷, catalysis⁸ and superconductivity⁹. Among the MXene family, titanium carbide (Ti₃C₂T_x), where T_x are the surface groups typically composed of O, OH or F, is the most investigated composition, while other compositions have been continuously developed¹⁰, along with new synthesis approaches and surface chemistry controls^{9,11,12}.

In recent years, MXenes have also gained attention for their potential use in light-to-heat conversion systems. Metallic MXenes based on Ti₃C₂T_x have shown high efficiency in converting sunlight into heat, with some studies reporting efficiencies approaching 100%^{13,14}. This has made MXenes attractive for use in solar-powered water evaporation¹⁵ and photothermal actuators¹⁶. In addition, MXenes with efficient photothermal properties have been explored as potential phototherapy agents for treating tumors by localizing heat on specific biological tissues^{17–19}. To engineer the photothermal properties of MXenes for these applications, it is important to understand fundamental light-to-heat conversion processes involving electron-phonon couplings, as well as thermal relaxation involving phonon-phonon couplings. Despite prior studies on thermal^{19–26} and thermoelectric^{27,28} properties, nonequilibrium photothermal processes and their associated microscopic couplings in the MXenes have remained mostly elusive.

In this study, we performed time-resolved electron and X-ray diffraction on thin films of $Ti_3C_2T_x$ ($T_x = O$, OH, F) and $Ti_3C_2Cl_2$ MXenes to study photoinduced heating and subsequent cooling responses at ultrafast timescales. Upon femtosecond laser pulse excitation, MXene thin

films heat up with an extremely fast response time on the order of a few hundred femtoseconds arising from strong electron-phonon coupling strength reaching $2.7 \cdot 10^{18} \, W \, m^{-3} K^{-1}$. This strong electron-phonon coupling is two orders of magnitude larger than that of conventional metals such as gold and silver²⁹, and it largely contributes to the high efficiency of light-to-heat conversion. By probing thermal relaxation on nanosecond timescales, we also uncover how MXene thin films dissipate heat. We show that the thermal boundary conductance (TBC) of the MXene-substrate interface plays a key role in determining thermal dissipation in samples thinner than the optical penetration depth. In $T_{13}C_2T_x$, we estimate the TBC to be approximately 10 MW m⁻² K⁻¹, which is at least one order of magnitude lower than that of typical metal-dielectric interfaces, but comparable to that of other 2D van der Waals materials³⁰. Through a systematic investigation of sample properties, we uncovered that the TBC can be doubled up to 20 MW m⁻² K⁻¹ by using smaller MXene flakes or chloride surface termination suggesting new thermal management strategies in photothermal, plasmonic, and thermoelectric applications.

We first present the results from ultrafast electron diffraction (UED) experiments performed at the MeV-UED instrument³¹ at the SLAC National Laboratory (see SI-Section S1). We collected electron diffraction in a transmission mode (Figure 1a) from $Ti_3C_2T_x$ thin films that are prepared on SiN_x membranes (see SI-Section S2). The electron beam size was ~100 µm which probed multiple flakes with varying in-plane orientation, resulting in Debye-Scherrer rings on an area detector (Figure 1a). We obtained the diffractogram, I(Q), by azimuthal integration of the diffraction images (Figure 1b), and labeled the (hkl) reflections on a thicker film sample, which showed a high degree of preferred orientation. This is evidenced by the large intensity of the inplane (110) peak in contrast to out-of-plane (00l) reflections indicating that the 2D planes lie mostly parallel to the surface of the SiN_x (see SI-Section 3). (10l) and (20l) peaks were also observed with a relatively weak intensity³². We also studied a thinner sample, which showed a complete 2D orientation, as the out-of-plane Bragg reflections were absent (see SI-Section 3).

We monitored transient changes in the diffractogram before and after laser excitation, as a function of the pump-probe delay (τ) . When τ is a few picoseconds, the intensity of the diffraction peaks decreases, corresponding to negative differential intensity $\Delta I(\tau = 5 \ ps)$ around the Bragg peaks (Figure 1b). The decrease in peak intensities indicates that the structure of

 $Ti_3C_2T_x$ becomes transiently disordered after excitation. To note, the disordering response fully recovers within 2.7 ms, which is the repetition period of the pump and probe pulses.

To understand the origin of the transient structural disordering, we plot transient logarithmic diffraction intensity (-log (I(Q))) across different reflections against the squared magnitude of the scattering vector (Q^2) in Figure 1c for the thicker sample where we can access multiple Bragg peaks. To improve the signal-to-noise in this analysis, we averaged measurements with pump-probe delays between 2 to 60 ps, where the response is flat (Figure S9). We observe a linear relationship between -log $(I(Q,\tau))$ and Q^2 which suggests that the transient structural response can simply be explained by a Debye-Waller (DW) model³³. This model manifests that any material, when heated up, would exhibit smaller diffraction peak intensity due to thermally-induced vibrations, and this effect is more pronounced for peaks at higher Q (SI-Section 4). Agreement with a DW model implies that the MXene flakes transiently disorder due to increased mean squared atomic displacements, and the UED data directly encodes the heating timescale of the MXene flakes.

Next, we estimate the strength of the electron-phonon coupling using a two-temperature model (TTM). For this we used measurements from the thinner sample, which could be homogeneously excited along the thickness direction and would not show saturable absorption effects^{34,35} at the given excitation density. We fit the rise time of the differential diffraction intensity measured at the (110) reflection (Figure 1d). The (110) peak is chosen as it exhibits the highest signal-to-noise ratio for the transient response, while other Bragg peaks show similar dynamics (Figure S8). By fitting the rise time, we obtained a time constant of 320 \pm 36 fs, denoting the lattice heating time, $\tau_{heating}$. The TTM interrelates $\tau_{heating}$ to the electron-phonon coupling by considering energy transfer from hot electrons to the atomic lattice (see SI-Section 4). We estimate g_{e-ph} to be 2.71 \cdot 10¹⁸ W $m^{-3}K^{-1}$ (see Section SI for the details of the calculation)

The value of g_{e-ph} in Ti₃C₂T_x is two orders of magnitude larger than that of conventional metals such as gold, silver and platinum^{29,36}. Also, the lattice heating time is significantly faster than that of semiconductor materials under similar excitation densities. For example, 2D materials such as MoS₂ and MoSe₂ have shown lattice heating time on the order of a picosecond^{33,37}, while II-VI semiconductors and lead halide perovskites have shown much

slower lattice heating on the order of a few to 10 ps^{38,39}. Thus, Ti₃C₂T_x exhibit a significantly fast light-to-heat conversion as compared to most conventional metals and semiconductors. Although the value of g_{e-ph} in Ti₃C₂T_x is large, it is comparable to that of d-block transition metals²⁹ such as Ti and Fe, with g_{e-ph} on the order of $1 - 4 \cdot 10^{18}$ W $m^{-3}K^{-1}$. As the 3d orbitals of titanium constitute most of the conduction band states above the Fermi level in Ti₃C₂T_x^{40,41}, our finding suggests that the strong electron-phonon coupling in Ti₃C₂T_x may be closely linked with the presence of titanium with intrinsically large g_{e-ph} . Similarly, first principles calculations⁴² have predicted a large g_{e-ph} of ~10¹⁸ W $m^{-3}K^{-1}$ in titanium nitride. Recent reports also indicate that strong electron-phonon coupling can be a common property among other MXenes comprising transition metals such as Mo⁴³, Nb⁴⁴ and Cr⁴⁵.

We used the experimentally determined value of g_{e-ph} to estimate $\tau_{heating}$ at varying excitation density using the TTM. As the electron temperature decreases with decreasing optical excitation fluence, the effective electron heat capacity also decreases, leading to a shorter $\tau_{heating}$. For instance, we estimated $\tau_{heating}$ to be ~125 fs for an excitation density of 1 mJ cm⁻² which agrees within a factor of 2 with the result of Volkov *et al.*⁴⁶ under the same fluence. To note, recent reports performing transient absorption on Ti₃C₂T_x have attributed the dynamic optical response on the order of few hundred femtoseconds to solely electron-electron scattering^{47,48}. However, our measurements unambiguously show that the electron-phonon coupling plays an important role in the early time dynamics, hence its contribution cannot be disregarded in the ultrafast optical response.

Strong scattering of electrons with phonons in Ti₃C₂T_x implies that the photoexcited hot carriers can transfer their kinetic energy to the atomic lattice very rapidly and efficiently without any loss such as due to hot electron radiative emission⁴⁹. Therefore, the strong electron-phonon coupling together with large, broadband light absorption of Ti₃C₂T_x MXenes are key factors contributing to their high efficiency in light-to-heat conversion. The ultrafast lattice heating response in Ti₃C₂T_x can enable new functionalities in photonic, catalytic and sensing applications by capitalizing on the extremely fast light-to-heat transduction. For example, ultrafast photoinduced strain may be used in optomechanical applications. Also, fast thermal conversion may empower unusual photo-thermo-catalytic functionalities^{50,51}. Additionally, plasmon-phonon coupling may allow ultrafast modulation of optical properties and may enable

sub-picosecond photothermal switches. In accordance with this, ultrafast modulation of terahertz radiation has been reported using the photoexcited Ti₃C₂T_x MXenes⁵².

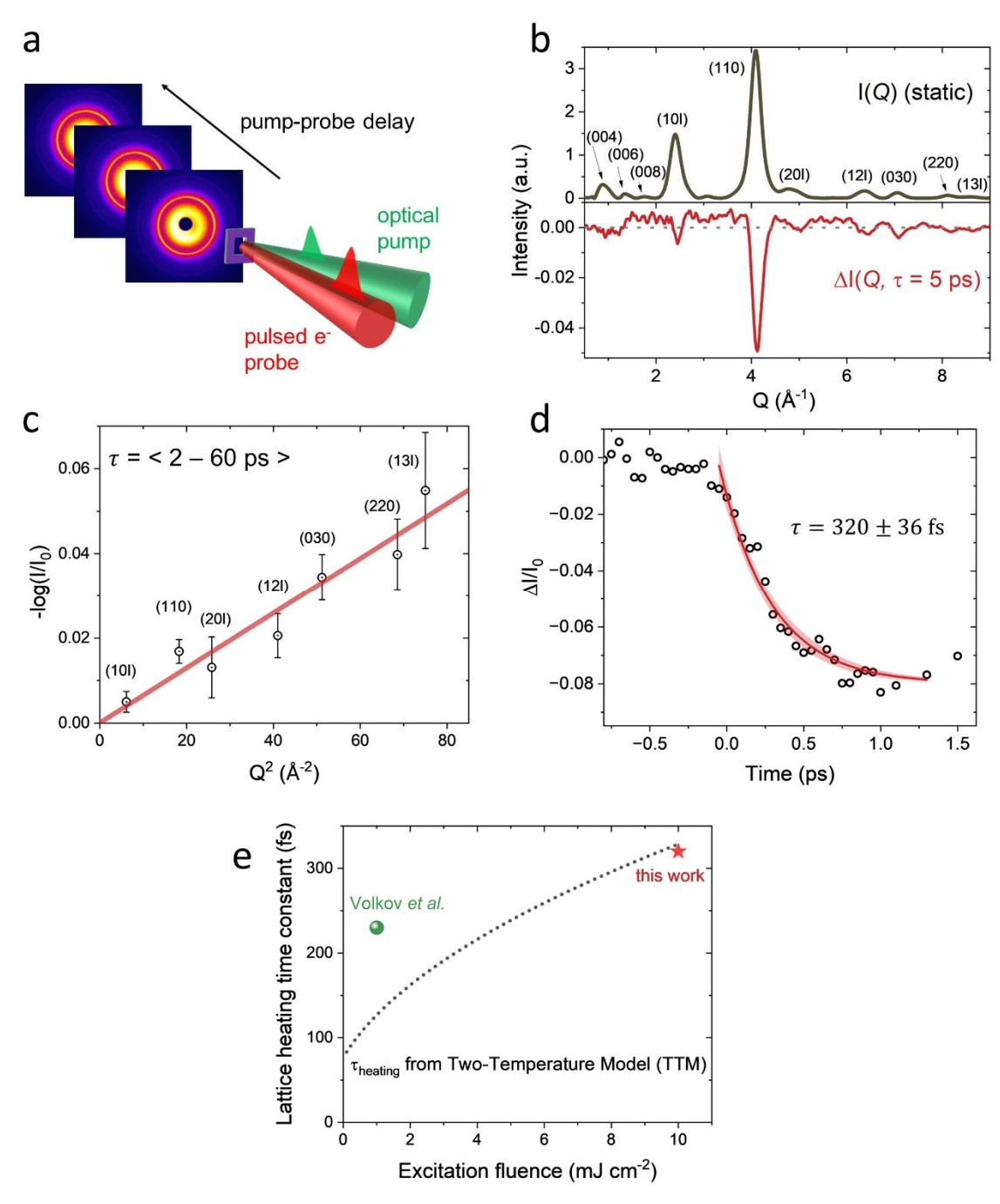


Figure 1. (a) Schematic of the pulsed optical pump / electron diffraction probe experiments performed in a transmission geometry. (b) Static diffraction intensity (I(Q)) in black with the Bragg peaks labeled. Inplane Bragg reflections dominate as the 2D layers are parallel to the SiN_x membrane. Transient differential diffraction intensity $(\Delta I(Q,\tau))$ in red showing decrease of the peak intensities. (c) Logarithmic normalized diffraction intensity $-ln(I/I_0)$ over the square of the reciprocal vector Q^2 showing a linear relationship consistent with a Debye-Waller model measured in a thicker UED film. (d)

Transient lattice heating response measured at (110) reflections showing a lattice heating time constant of 320 fs in a thinner UED film. (e) Lattice heating time estimated through a two-temperature model as a function of excitation density. Red star is the experimental data from this work and green dot is from Volkov et al.⁴⁶.

Now we turn our focus to thermal relaxation in photoexcited $T_{i3}C_2T_x$ thin films. Our UED data shows recovery of diffraction intensity, hinting thermal relaxation (Figure S9). While we can partly resolve the thermal relaxation in thinner (a few monolayer thick) MXene sample (Figure S9a), the relaxation in a thicker sample is beyond the maximum delay range of the UED (Figure S9b). To investigate thermal relaxation in samples with varying thickness and systematically study thermal relaxation pathways, we used pump-probe X-ray diffraction (XRD) conducted at the Beamline 11-ID-D of the Advanced Photon Source (SI-Section 5). Pump-probe XRD has been recently used to investigate thermal relaxation in thin films and buried interfaces, providing an all-optical non-invasive access to the sub-nanosecond thermal responses^{53,54}. Here, we carried out the transient XRD in a reflection geometry (Figure 2a) on MXene samples (SI-Section 2) that were spin-coated on substrates that are commonly used in applications. These samples exhibit complete 2D preferred orientation, as we can only resolve only the out-of-plane (00*l*) peaks (Figure S10). We track the position of (002) reflection in the reciprocal space, which encodes the sample temperature though a transient lattice expansion response. Figure 2b shows the probed (002) reflection at Q of 0.46 Å^{-1} , and the photoinduced changes presented by differential intensity $\Delta I(Q,\tau)$ measured at varying pump-probe delays. $\Delta I(Q,\tau)$ exhibits a derivative-like shape indicating a shift of the (002) reflection transiently towards low Q after the photoexcitation. This observation indicates that the MXene film expands along the surface normal direction due to photoinduced heating.

Figure 2c shows the transient lattice expansion quantified as $\Delta Q/Q_0$, measured for varying excitation fluences. To correlate transient lattice expansion with the actual sample temperature, we performed temperature dependent XRD measurements in the same diffraction configuration at the Beamline 7-ID-C. Figure 2d shows $\Delta Q/Q_0$ for (002) reflection measured for temperatures ranging from 200 to 340 K. Based on this calibration, we estimate an out-of-plane thermal expansion coefficient $\alpha = 2.25 \cdot 10^{-5} \text{ K}^{-1}$, which we use to convert the transient lattice expansion, $\Delta Q/Q_0$, into a differential sample temperature, ΔT . Figure 2e plots $\Delta T(\tau)$ for an optical excitation density of 0.8 mJ cm⁻², showing an initial temperature jump as high as 120 K, consistent with the absorbed energy density and the lattice heat capacity (SI-Section 4).

Figure 2f depicts the thermal relaxation time constant $\tau_{cooling}$ and the maximum temperature jump ΔT_{max} as a function of excitation fluence in a Ti₃C₂T_x thin film (thickness: 12 nm) on sapphire. $\tau_{cooling}$ is obtained by fitting the data in Figure 2c with a single exponential function. The fits resulted in a coefficient of determination (i.e., R^2) of 0.96-0.97. Although we could obtain $R^2 \sim 0.99$ by using double exponential or stretched exponential functions, it then becomes ambiguous to define $\tau_{cooling}$. Therefore, we decided to keep single exponential function fitting for all samples for the sake of simple interpretation of $\tau_{cooling}$ relative to varying sample properties, e.g., thickness. In the thin film with a thickness of 12 nm, $\tau_{cooling}$ is approximately 2 ns, independent of the excitation fluence (Figure 2f). Thus, the cooling time is independent of the absorbed energy density, hence the photoinduced temperature jump, ΔT_{max} . On the other hand, ΔT_{max} itself scales linearly with the excitation fluence, as the absorbed optical energy scales linearly with the excitation fluence. It is worth noting that the samples were extremely stable under both laser and X-ray pulses, as shown by no change in diffraction intensity over 2.5 hours of data acquisition (Figure S11).

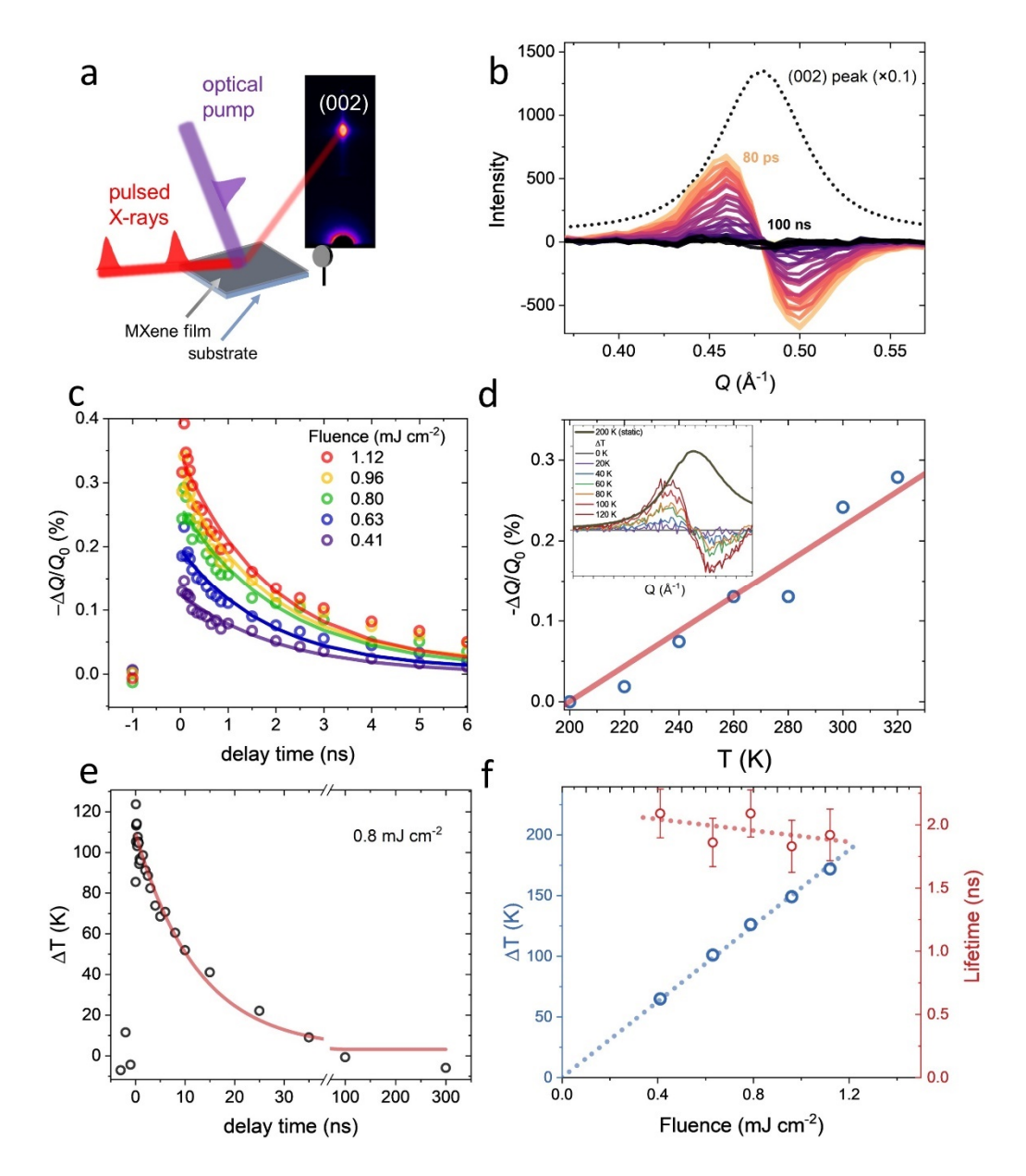


Figure 2. (a) Schematic of the optical pump – X-ray diffraction probe measurements. The X-ray diffraction is in forward reflection mode collected by a large area detector. Optical pump is surface normal to the sample. (b) Diffractogram showing (002) reflection in dotted black and transient differential intensity measured at various pump-probe delays in solid colors from yellow to black. Differential intensity response indicates a shift of (002) peak to lower Q due to lattice expansion. The sample used for this figure is $Ti_3C_2T_x$ (T=0, OH and F surface groups) with a film thickness of 12 nm prepared on sapphire. (c) Excitation fluence dependent transient lattice expansion response at the (002). Data is obtained by Gaussian fitting of the (002) peak as a function of pump-probe delay. Decay curves are fitted by a single exponential function. (d) Static temperature dependent measurement of lattice expansion. (e) Transient temperature jump vs. pump-probe delay. (f) Temperature jump and thermal relaxation lifetime as a function of excitation fluence.

We investigate the relationship between $\tau_{cooling}$ and the film thickness. For this, we prepared samples with thicknesses ranging from 7 to 52 nm and measured their transient responses with single exponential fits (Figure 3a). Figure 3b shows the fitted $\tau_{cooling}$. For sample thicknesses up to 40 nm, there is a linear relationship between the sample thickness, L, and the cooling time constant, while the thickest sample (L = 52 nm) clearly deviates from linearity. To estimate $\tau_{cooling}$ in thin samples (\leq 40 nm), we use a simple RC circuit model that considers the volumetric heat capacity, C_v , of the MXene thin film and the thermal boundary conductance (TBC), denoted as G, also known as the Kapitza conductance, across the MXene-substrate interface. In this model, the thermal relaxation time is equal to the RC time constant $\tau_{cooling} =$ $C_v L = \frac{1}{G}$. Using this, we estimate the G (black squares Figure 3c). On average, G is 9.2 \pm $0.8 \ MW \ m^{-2} \ K^{-1}$ for the $Ti_3C_2T_x$ thin films ($L < 40 \ nm$) on sapphire, which is in good agreement with a prior report²¹, as shown by the red square in Figure 3c. The RC circuit model assumes a homogenously heated slab thermally relaxing via the TBC. The photoinduced temperature jump would be homogeneous only for samples thinner than the optical penetration depth (SI-Section 4), which agrees with the linear region in Figure 3c. For samples much thicker than the optical penetration depth, thermal transport within the film itself starts to play an important play role. Therefore, thermal relaxation becomes a convolution of heat transfer across the MXene layers as well as the MXene-substrate interface.

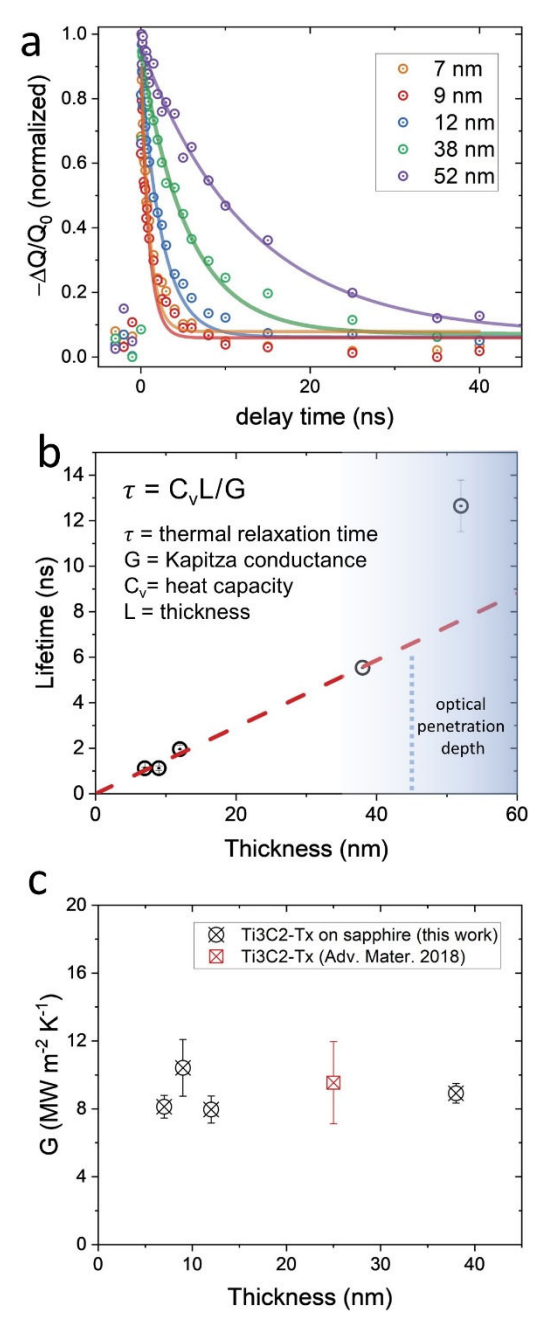


Figure 3. (a) Normalized lattice expansion response in MXenes films with varying thickness. Cooling lifetimes are fitted by a single exponential decay function. (b) Film thickness vs. fitted thermal relaxation lifetime showing a linear dependence for sample thickness up to 40 nm. Dotted line indicates that position of the optical penetration depth. (c) Sample thickness dependent TBC measurement. Black squares represent data from our measurements. Red square is from Yasaei *et al.*²¹

The TBC of the MXene-sapphire interface ($G \sim 9.2~MW~m^{-2}~K^{-1}$) is small as compared to those of conventional metals such as Pt/sapphire ($G \sim 140~MW~m^{-2}~K^{-1}$) and Al/Si

 $(G \sim 190~MW~m^{-2}~K^{-1})$. This indicates that the thermal relaxation of MXene thin film is impeded due to weak interfacial thermal conductance, or high Kapitza resistance⁵⁵. The small TBC in MXenes is in close resemblance³⁰ to those of other van der Waals materials such as the transition metal dichalcogenides (e.g., MoS₂) with G on the order of 20 $MW~m^{-2}~K^{-1}$. In 2D systems, flexural phonons involving out-of-plane bending/buckling of 2D layers have been suggested to mediate cross-plane heat transfer⁵⁶. Nevertheless, acoustic mismatch of the flexural modes with the longitudinal phonon modes of substrates typically impedes the cross-plane thermal transport. As a result, understanding and controlling interfacial thermal transport in 2D materials has become an active area of research in recent years^{30,53,57}.

We explored how various sample attributes affect the TBC in Ti₃C₂-based MXenes by taking advantage of the pump-probe XRD enabling access to the TBC independent of the sample type. We investigated the effects of sample annealing temperature, substrate type, lateral flake size and chemical surface termination. Figure 4 demonstrates the experimentally measured TBCs for the corresponding sample types.

Ti₃C₂T_x (T_x = O, OH, F) MXene films with large flake size on sapphire show an average $G = 9.2 \, MW \, m^{-2} \, K^{-1}$ when they were annealed at 300 °C. In comparison, the non-annealed samples show a reduced G of 7.8 $MW \, m^{-2} \, K^{-1}$ which suggests that the annealing could slightly improve G. Previous work by Hart $et \, al$. have shown that electrical conductivity of the MXenes can be significantly improved by annealing⁵⁸. Consistent with this, we observed an improvement in the sheet resistance of the annealed MXene films (see SI-Section 6). On the other hand, the enhancement of the TBC is ~10%, indicating that annealing at 300°C does not considerably alter the MXene-substate interface. Hemmat $et \, al$. ²² have suggested that annealing at temperatures beyond 300°C could further improve the thermal conductivity of MXenes by removal of -O and -OH surface species.

To probe the substrate effect, we studied MXene films on sapphire, silicon and glass with the same film attributes (large flake size, T_x surface termination, and annealed at 300°C). We find that G is the largest on sapphire. On silicon, G is 4.5 MW m^{-2} K^{-1} , which is ~50% smaller than that of sapphire. This observation indicates that the interfacial coupling between the MXene and sapphire is stronger than that between MXene and silicon, leading to a better cross-plane

vibrational matching. A similar observation has been made for graphene/sapphire vs. graphene/silicon interfaces⁵⁹.

Next, we compared the effect of lateral flake size and surprisingly found a strong enhancement of G in samples with smaller lateral flake size (< 100 nm). These samples consistently show a large G of about 19.5 MW m^{-2} K^{-1} , which is a factor of 2 larger than that of samples with large flake size (400 nm ± 200 nm). Smaller flake Ti₃C₂T_x on silicon also shows G of $\sim 16 \ MW \ m^{-2} \ K^{-1}$ that is 3-fold larger than its large-flake counterpart. The lateral flake size dependence has been investigated in 2D materials for their in-plane thermal transport, where flakes with sizes larger than the phonon mean free path have been shown to maximize the inplane thermal transport⁶⁰. However, the effect of lateral flake size on the cross-plane thermal transport has not been well understood. Our observation indicates that the TBC in MXenes can be improved by using smaller flakes which can be understood by multiple hypotheses. Structural defects arising from surface pinning and wrinkling may play a role here, as these have been shown to impede the flexural phonons, hence limiting the cross-plane heat dissipation⁶¹. Supporting this hypothesis, temperature mapping in MXenes has shown that wrinkled and pinned regions can trap heat, causing hot spot formation²³. Therefore, smaller flake MXenes with smaller density of defects may exhibit improved interfacial thermal coupling. In addition to structural defects, other factors could be contributing. One such factor is the contribution of the edges of the flakes to the cross-plane thermal transport⁶². Moreover, variation in the trapped surface moieties with varying flake size could also play a role. Strong electron-phonon coupling may further influence the flake size dependence of the TBC^{44,63,64}. Large flake samples show an order of magnitude smaller sheet resistance compared to small flake ones (see Figures S6 and S7). The increased electron density resulting in an increased electron-phonon scattering may decrease the TBC in in large flake MXenes. Further investigations are necessary to better understand the flake-size-dependent thermal properties in MXenes.

In our final investigation, we studied the effect of chemical surface termination on the TBC. For this, we synthesized Ti₃C₂Cl₂ MXenes using Lewis acidic molten salt etching method⁶⁵. This approach allows the transformation of Ti₃AlC₂ MAX phase into Ti₃C₂Cl₂ MXene, and exchange of chloride surface groups with chalcogens and other surface groups as our team has recently developed⁹. We find that large flake Ti₃C₂Cl₂ thin films exhibit G of 20 MW m^{-2} K^{-1} showing

approximately 2-fold enhancement in contrast to the same samples with mixed T_x surface terminations. This enhancement of the TBC via a surface chemistry control has been predicted by first-principle modeling^{24,26}. Theoretically, pure halide termination (e.g., -F) has been suggested to improve thermal conductivity as compared to -O and -OH terminations. Our experiments corroborate this prediction and show that pure halide, i.e., chloride, surface termination can strongly improve the TBC. Therefore, our results indicate that surface chemistry can be a versatile tool to manipulate thermal properties of MXenes, presenting opportunities in photothermal and thermoelectric applications.

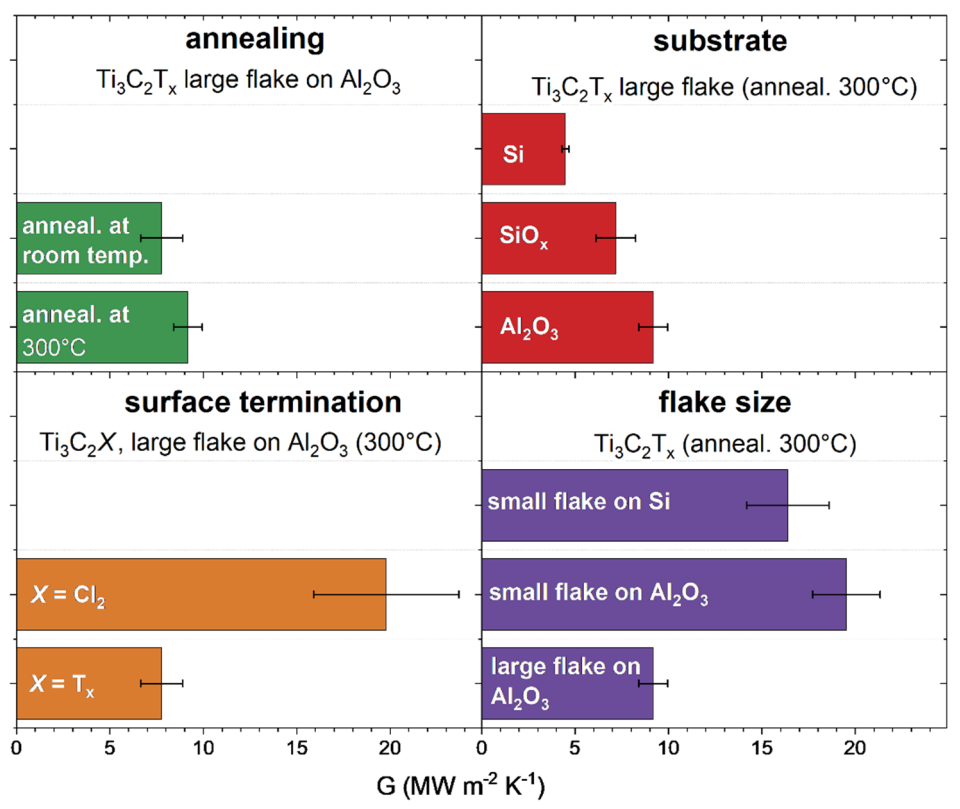


Figure 4. Measured TBC for different sample attributes: flake size (large vs. small), surface termination (- T_x vs. -Cl), substrate (sapphire, silicon and glass), annealing temperature (300°C vs. 25°C).

Overall, MXenes can convert light into heat much faster than most other materials due to their strong electron-phonon coupling. In addition, slow thermal dissipation enables the MXenes to store heat for a prolonged period of time. The combination of a large electron-phonon coupling and slow interfacial thermal transport makes them appealing for various applications ranging from photothermal therapy and solar steam generation to thermoelectrics and photothermal catalysis.

In summary, we have used ultrafast electron and X-ray probes to investigate how MXene films heat and subsequently cool under pulsed optical excitation. Our experiments provide valuable insights into the fundamental electron-phonon and phonon-phonon couplings in Ti₃C₂-based MXenes which govern their lattice heating and cooling dynamics. By studying various sample attributes, we uncover the effects of lateral flake size and chemical surface termination on the thermal boundary conductance, providing new insights into engineering photothermal properties of MXenes. Also, ultrafast thermal responses in MXenes uncovered here may inspire new applications harnessing sub-picosecond light-to-heat transduction capabilities in areas such as photonics and photocatalysis. As a future direction, we envision using ultrafast structural probes combined with real-space imaging capabilities to map thermal transport in 2D materials and their devices, empowering a thorough understanding of these emerging material systems.

ACKNOWLEDGEMENTS

This research used resources of the Advanced Photon Source and the Center for Nanoscale Materia, U.S. Department of Energy (DOE) Office of Science User Facilities, operated for the DOE Office of Science by Argonne National Laboratory under Contract No. DE-AC02-06CH11357. Extraordinary facility operations were supported in part by the DOE Office of Science through the National Virtual Biotechnology Laboratory, a consortium of DOE national laboratories focused on the response to COVID-19, with funding provided by the Coronavirus CARES Act. MeV-UED is operated as part of the Linac Coherent Light Source at the SLAC National Accelerator Laboratory, supported by the U.S. Department of Energy, Office of Science, Office of Basic Energy Sciences under Contract No. DE-AC02-76SF00515. The work on MXene synthesis was supported by the National Science Foundation under award number DMR-2004880 and surface functionalization studies were supported by the Department of Defense Air Force Office of Scientific Research under grant numbers FA9550-22-1-0283 and DURIP FA9550-20-1-0104. This project also used facilities supported of the University of Chicago Materials Research Science and Engineering Center, which is funded by the National Science Foundation under award number DMR-2011854. A.M.L. acknowledges support from the Department of Energy, Office of Science, Basic Energy Sciences, Materials Sciences and Engineering Division, under Contract DE-AC02-76SF00515.

AUTHOR DECLARATIONS

Conflict of Interest

The authors have no conflict of interest to disclose.

DATA AVAILABLITY

The data that support the findings of this study are available from the corresponding author upon reasonable request.

SUPPORTING INFORMATION

Supporting information containing information on experimental details for MXene synthesis, sample preparation and characterization, ultrafast electron diffraction, pump-probe X-ray diffraction, two-temperature model.

REFERENCES

- (1) Naguib, M.; Kurtoglu, M.; Presser, V.; Lu, J.; Niu, J.; Heon, M.; Hultman, L.; Gogotsi, Y.; Barsoum, M. W. Two-Dimensional Nanocrystals Produced by Exfoliation of Ti3AlC2. *Adv. Mater.*, **2011**, *23*, 4248–4253.
- (2) Naguib, M.; Mochalin, V. N.; Barsoum, M. W.; Gogotsi, Y. 25th Anniversary Article: MXenes: A New Family of Two-Dimensional Materials. *Adv. Mater.*, **2014**, *26*, 992–1005.
- (3) Fu, Z.; Wang, N.; Legut, D.; Si, C.; Zhang, Q.; Du, S.; Germann, T. C.; Francisco, J. S.; Zhang, R. Rational Design of Flexible Two-Dimensional MXenes with Multiple Functionalities. *Chem. Rev.*, **2019**, *119*, 11980–12031.
- (4) Lipatov, A.; Alhabeb, M.; Lukatskaya, M. R.; Boson, A.; Gogotsi, Y.; Sinitskii, A. Effect of Synthesis on Quality, Electronic Properties and Environmental Stability of Individual Monolayer Ti 3 C 2 MXene Flakes. *Adv. Electron. Mater.*, **2016**, *2*, 1600255.
- (5) Halim, J.; Lukatskaya, M. R.; Cook, K. M.; Lu, J.; Smith, C. R.; Näslund, L.-Å.; May, S. J.; Hultman, L.; Gogotsi, Y.; Eklund, P.; Barsoum, M. W. Transparent Conductive Two-

- Dimensional Titanium Carbide Epitaxial Thin Films. Chem. Mater., 2014, 26, 2374–2381.
- (6) Shahzad, F.; Alhabeb, M.; Hatter, C. B.; Anasori, B.; Man Hong, S.; Koo, C. M.; Gogotsi, Y. Electromagnetic Interference Shielding with 2D Transition Metal Carbides (MXenes). *Science*, 2016, 353, 1137–1140.
- (7) Pang, J.; Mendes, R. G.; Bachmatiuk, A.; Zhao, L.; Ta, H. Q.; Gemming, T.; Liu, H.; Liu, Z.; Rummeli, M. H. Applications of 2D MXenes in Energy Conversion and Storage Systems. *Chem. Soc. Rev.*, **2019**, *48*, 72–133.
- (8) Zhang, J.; Zhao, Y.; Guo, X.; Chen, C.; Dong, C.-L.; Liu, R.-S.; Han, C.-P.; Li, Y.; Gogotsi, Y.; Wang, G. Single Platinum Atoms Immobilized on an MXene as an Efficient Catalyst for the Hydrogen Evolution Reaction. *Nat. Catal.*, **2018**, *1*, 985–992.
- (9) Kamysbayev, V.; Filatov, A. S.; Hu, H.; Rui, X.; Lagunas, F.; Wang, D.; Klie, R. F.; Talapin, D. V. Covalent Surface Modifications and Superconductivity of Two-Dimensional Metal Carbide MXenes. *Science*, 2020, 369, 979–983.
- (10) Lim, K. R. G.; Shekhirev, M.; Wyatt, B. C.; Anasori, B.; Gogotsi, Y.; Seh, Z. W. Fundamentals of MXene Synthesis. *Nat. Synth.*, **2022**, *1*, 601–614.
- (11) Shekhirev, M.; Busa, J.; Shuck, C. E.; Torres, A.; Bagheri, S.; Sinitskii, A.; Gogotsi, Y. Ultralarge Flakes of Ti3C2Tx MXene via Soft Delamination. *ACS Nano*, **2022**, *16*, 13695–13703.
- (12) Shao, Y.; Wei, L.; Wu, X.; Jiang, C.; Yao, Y.; Peng, B.; Chen, H.; Huangfu, J.; Ying, Y.; Zhang, C. J.; Ping, J. Room-Temperature High-Precision Printing of Flexible Wireless Electronics Based on MXene Inks. *Nat. Commun.*, **2022**, *13*, 3223.
- (13) Li, R.; Zhang, L.; Shi, L.; Wang, P. MXene Ti 3 C 2: An Effective 2D Light-to-Heat Conversion Material. *ACS Nano*, **2017**, *11*, 3752–3759.
- (14) Gao, M.; Zhu, L.; Peh, C. K.; Ho, G. W. Solar Absorber Material and System Designs for Photothermal Water Vaporization towards Clean Water and Energy Production. *Energy Environ. Sci.*, **2019**, *12*, 841–864.
- (15) Xu, D.; Li, Z.; Li, L.; Wang, J. Insights into the Photothermal Conversion of 2D MXene

- Nanomaterials: Synthesis, Mechanism, and Applications. *Adv. Funct. Mater.*, **2020**, *30*, 2000712.
- (16) Cao, W.-T.; Feng, W.; Jiang, Y.-Y.; Ma, C.; Zhou, Z.-F.; Ma, M.-G.; Chen, Y.; Chen, F. Two-Dimensional MXene-Reinforced Robust Surface Superhydrophobicity with Self-Cleaning and Photothermal-Actuating Binary Effects. *Mater. Horizons*, 2019, 6, 1057–1065.
- (17) Lin, H.; Gao, S.; Dai, C.; Chen, Y.; Shi, J. A Two-Dimensional Biodegradable Niobium Carbide (MXene) for Photothermal Tumor Eradication in NIR-I and NIR-II Biowindows. *J. Am. Chem. Soc.*, **2017**, *139*, 16235–16247.
- (18) Lin, H.; Wang, Y.; Gao, S.; Chen, Y.; Shi, J. Theranostic 2D Tantalum Carbide (MXene). *Adv. Mater.*, **2018**, *30*, 1703284.
- (19) Yu, L.; Xu, L.; Lu, L.; Alhalili, Z.; Zhou, X. Thermal Properties of MXenes and Relevant Applications. *ChemPhysChem*, **2022**, *23*, e20220020.
- (20) Chen, L.; Shi, X.; Yu, N.; Zhang, X.; Du, X.; Lin, J. Measurement and Analysis of Thermal Conductivity of Ti3C2Tx MXene Films. *Materials (Basel).*, **2018**, *11*, 1701.
- (21) Yasaei, P.; Hemmat, Z.; Foss, C. J.; Li, S. J.; Hong, L.; Behranginia, A.; Majidi, L.; Klie, R. F.; Barsoum, M. W.; Aksamija, Z.; Salehi-Khojin, A. Enhanced Thermal Boundary Conductance in Few-Layer Ti3C2 MXene with Encapsulation. *Adv. Mater.*, **2018**, *30*, 1801629.
- (22) Hemmat, Z.; Yasaei, P.; Schultz, J. F.; Hong, L.; Majidi, L.; Behranginia, A.; Verger, L.; Jiang, N.; Barsoum, M. W.; Klie, R. F.; Salehi-Khojin, A. Tuning Thermal Transport Through Atomically Thin Ti3C2Tz MXene by Current Annealing in Vacuum. *Adv. Funct. Mater.*, **2019**, *29*, 1805693.
- (23) Yasaei, P.; Tu, Q.; Xu, Y.; Verger, L.; Wu, J.; Barsoum, M. W.; Shekhawat, G. S.; Dravid, V. P. Mapping Hot Spots at Heterogeneities of Few-Layer Ti3C2 MXene Sheets. *ACS Nano*, **2019**, *13*, 3301–3309.
- (24) Gholivand, H.; Fuladi, S.; Hemmat, Z.; Salehi-Khojin, A.; Khalili-Araghi, F. Effect of Surface Termination on the Lattice Thermal Conductivity of Monolayer Ti3C2Tz

- MXenes. J. Appl. Phys., 2019, 126, 065101.
- (25) Zha, X.-H.; Yin, J.; Zhou, Y.; Huang, Q.; Luo, K.; Lang, J.; Francisco, J. S.; He, J.; Du, S. Intrinsic Structural, Electrical, Thermal, and Mechanical Properties of the Promising Conductor Mo2C MXene. J. Phys. Chem. C, 2016, 120, 15082–15088.
- (26) Guo, Z.; Miao, N.; Zhou, J.; Pan, Y.; Sun, Z. Coincident Modulation of Lattice and Electron Thermal Transport Performance in MXenes via Surface Functionalization. *Phys. Chem. Chem. Phys.*, 2018, 20, 19689–19697.
- (27) Lu, X.; Zhang, Q.; Liao, J.; Chen, H.; Fan, Y.; Xing, J.; Gu, S.; Huang, J.; Ma, J.; Wang, J.; Wang, L.; Jiang, W. High-Efficiency Thermoelectric Power Generation Enabled by Homogeneous Incorporation of MXene in (Bi,Sb)2Te3 Matrix. Adv. Energy Mater., 2020, 10, 1902986.
- (28) Kim, H.; Anasori, B.; Gogotsi, Y.; Alshareef, H. N. Thermoelectric Properties of Two-Dimensional Molybdenum-Based MXenes. *Chem. Mater.*, **2017**, *29*, 6472–6479.
- (29) Medvedev, N.; Milov, I. Electron-Phonon Coupling in Metals at High Electronic Temperatures. *Phys. Rev. B*, **2020**, *102*, 064302.
- (30) Giri, A.; Hopkins, P. E. A Review of Experimental and Computational Advances in Thermal Boundary Conductance and Nanoscale Thermal Transport across Solid Interfaces. *Adv. Funct. Mater.*, **2020**, *30*, 1903857.
- (31) Weathersby, S. P.; Brown, G.; Centurion, M.; Chase, T. F.; Coffee, R.; Corbett, J.; Eichner, J. P.; Frisch, J. C.; Fry, A. R.; Gühr, M.; Hartmann, N.; Hast, C.; Hettel, R.; Jobe, R. K.; Jongewaard, E. N.; Lewandowski, J. R.; Li, R. K.; Lindenberg, A. M.; Makasyuk, I.; et al. Mega-Electron-Volt Ultrafast Electron Diffraction at SLAC National Accelerator Laboratory. *Rev. Sci. Instrum.*, 2015, 86, 073702.
- (32) Ghidiu, M.; Barsoum, M. W. The {110} Reflection in X-ray Diffraction of MXene Films: Misinterpretation and Measurement via Non-standard Orientation. J. Am. Ceram. Soc., 2017, 100, 5395–5399.
- (33) Mannebach, E. M.; Li, R.; Duerloo, K.-A.; Nyby, C.; Zalden, P.; Vecchione, T.; Ernst, F.; Reid, A. H.; Chase, T.; Shen, X.; Weathersby, S.; Hast, C.; Hettel, R.; Coffee, R.;

- Hartmann, N.; Fry, A. R.; Yu, Y.; Cao, L.; Heinz, T. F.; et al. Dynamic Structural Response and Deformations of Monolayer MoS2 Visualized by Femtosecond Electron Diffraction. *Nano Lett.*, **2015**, *15*, 6889–6895.
- (34) Jhon, Y. I.; Koo, J.; Anasori, B.; Seo, M.; Lee, J. H.; Gogotsi, Y.; Jhon, Y. M. Metallic MXene Saturable Absorber for Femtosecond Mode-Locked Lasers. *Adv. Mater.*, **2017**, *29*, 1702496.
- (35) Dong, Y.; Chertopalov, S.; Maleski, K.; Anasori, B.; Hu, L.; Bhattacharya, S.; Rao, A. M.; Gogotsi, Y.; Mochalin, V. N.; Podila, R. Saturable Absorption in 2D Ti 3 C 2 MXene Thin Films for Passive Photonic Diodes. *Adv. Mater.*, **2018**, *30*, 1705714.
- (36) Guzelturk, B.; Utterback, J. K.; Coropceanu, I.; Kamysbayev, V.; Janke, E. M.; Zajac, M.; Yazdani, N.; Cotts, B. L.; Park, S.; Sood, A.; Lin, M.-F.; Reid, A. H.; Kozina, M. E.; Shen, X.; Weathersby, S. P.; Wood, V.; Salleo, A.; Wang, X.; Talapin, D. V.; et al. Nonequilibrium Thermodynamics of Colloidal Gold Nanocrystals Monitored by Ultrafast Electron Diffraction and Optical Scattering Microscopy. *ACS Nano*, **2020**, *14*, 4792–4804.
- (37) Lin, M.-F.; Kochat, V.; Krishnamoorthy, A.; Bassman, L.; Weninger, C.; Zheng, Q.; Zhang, X.; Apte, A.; Tiwary, C. S.; Shen, X.; Li, R.; Kalia, R.; Ajayan, P.; Nakano, A.; Vashishta, P.; Shimojo, F.; Wang, X.; Fritz, D. M.; Bergmann, U. Ultrafast Non-Radiative Dynamics of Atomically Thin MoSe2. *Nat. Commun.*, **2017**, *8*, 1745.
- (38) Guzelturk, B.; Cotts, B. L.; Jasrasaria, D.; Philbin, J. P.; Hanifi, D. A.; Koscher, B. A.; Balan, A. D.; Curling, E.; Zajac, M.; Park, S.; Yazdani, N.; Nyby, C.; Kamysbayev, V.; Fischer, S.; Nett, Z.; Shen, X.; Kozina, M. E.; Lin, M.-F.; Reid, A. H.; et al. Dynamic Lattice Distortions Driven by Surface Trapping in Semiconductor Nanocrystals. *Nat. Commun.*, **2021**, *12*, 1860.
- (39) Wu, X.; Tan, L. Z.; Shen, X.; Hu, T.; Miyata, K.; Trinh, M. T.; Li, R.; Coffee, R.; Liu, S.; Egger, D. A.; Makasyuk, I.; Zheng, Q.; Fry, A.; Robinson, J. S.; Smith, M. D.; Guzelturk, B.; Karunadasa, H. I.; Wang, X.; Zhu, X.; et al. Light-Induced Picosecond Rotational Disordering of the Inorganic Sublattice in Hybrid Perovskites. *Sci. Adv.*, 2017, 3, e1602388.

- (40) Khazaei, M.; Ranjbar, A.; Arai, M.; Sasaki, T.; Yunoki, S. Electronic Properties and Applications of MXenes: A Theoretical Review. *J. Mater. Chem. C*, **2017**, *5*, 2488–2503.
- (41) Faraji, M.; Bafekry, A.; Fadlallah, M. M.; Molaei, F.; Hieu, N. N.; Qian, P.; Ghergherehchi, M.; Gogova, D. Surface Modification of Titanium Carbide MXene Monolayers (Ti2C and Ti3C2) via Chalcogenide and Halogenide Atoms. *Phys. Chem. Chem. Phys.*, 2021, 23, 15319–15328.
- (42) Dal Forno, S.; Lischner, J. Electron-Phonon Coupling and Hot Electron Thermalization in Titanium Nitride. *Phys. Rev. Mater.*, **2019**, *3*, 115203.
- (43) Zhang, Q.; Li, J.; Wen, J.; Li, W.; Chen, X.; Zhang, Y.; Sun, J.; Yan, X.; Hu, M.; Wu, G.; Yuan, K.; Guo, H.; Yang, X. Simultaneous Capturing Phonon and Electron Dynamics in MXenes. *Nat. Commun.*, **2022**, *13*, 7900.
- (44) Huang, Y.; Zhou, J.; Wang, G.; Sun, Z. Abnormally Strong Electron–Phonon Scattering Induced Unprecedented Reduction in Lattice Thermal Conductivity of Two-Dimensional Nb 2 C. J. Am. Chem. Soc., 2019, 141, 8503–8508.
- (45) Bekaert, J.; Sevik, C.; Milošević, M. V. First-Principles Exploration of Superconductivity in MXenes. *Nanoscale*, **2020**, *12*, 17354–17361.
- (46) Volkov, M.; Willinger, E.; Kuznetsov, D. A.; Müller, C. R.; Fedorov, A.; Baum, P. Photo-Switchable Nanoripples in Ti 3 C 2 T x MXene. *ACS Nano*, **2021**, *15*, 14071–14079.
- (47) Li, J.; Chi, Z.; Qin, R.; Yan, L.; Lin, X.; Hu, M.; Shan, G.; Chen, H.; Weng, Y.-X. Hydrogen Bond Interaction Promotes Flash Energy Transport at MXene-Solvent Interface. *J. Phys. Chem. C*, **2020**, *124*, 10306–10314.
- (48) Zhang, Q.; Yan, L.; Yang, M.; Wu, G.; Hu, M.; Li, J.; Yuan, K.; Yang, X. Ultrafast Transient Spectra and Dynamics of MXene (Ti3C2Tx) in Response to Light Excitations of Various Wavelengths. *J. Phys. Chem. C*, **2020**, *124*, 6441–6447.
- (49) Sivan, Y.; Dubi, Y. Theory of "Hot" Photoluminescence from Drude Metals. *ACS Nano*, **2021**, *15*, 8724–8732.
- (50) Meng, X.; Liu, L.; Ouyang, S.; Xu, H.; Wang, D.; Zhao, N.; Ye, J. Nanometals for Solar-

- to-Chemical Energy Conversion: From Semiconductor-Based Photocatalysis to Plasmon-Mediated Photocatalysis and Photo-Thermocatalysis. *Adv. Mater.*, **2016**, *28*, 6781–6803.
- (51) Dubi, Y.; Un, I. W.; Sivan, Y. Thermal Effects an Alternative Mechanism for Plasmon-Assisted Photocatalysis. *Chem. Sci.*, **2020**, *11*, 5017–5027.
- (52) Li, G.; Amer, N.; Hafez, H. A.; Huang, S.; Turchinovich, D.; Mochalin, V. N.; Hegmann, F. A.; Titova, L. V. Dynamical Control over Terahertz Electromagnetic Interference Shielding with 2D Ti3C2Ty MXene by Ultrafast Optical Pulses. *Nano Lett.*, 2020, 20, 636–643.
- (53) Nyby, C.; Sood, A.; Zalden, P.; Gabourie, A. J.; Muscher, P.; Rhodes, D.; Mannebach, E.; Corbett, J.; Mehta, A.; Pop, E.; Heinz, T. F.; Lindenberg, A. M. Visualizing Energy Transfer at Buried Interfaces in Layered Materials Using Picosecond X-Rays. *Adv. Funct. Mater.*, **2020**, *30*, 2002282.
- (54) Kozina, M.; Hu, T.; Wittenberg, J. S.; Szilagyi, E.; Trigo, M.; Miller, T. A.; Uher, C.; Damodaran, A.; Martin, L.; Mehta, A.; Corbett, J.; Safranek, J.; Reis, D. A.; Lindenberg, A. M. Measurement of Transient Atomic Displacements in Thin Films with Picosecond and Femtometer Resolution. *Struct. Dyn.*, 2014, 1, 034301.
- (55) Pollack, G. L. Kapitza Resistance. *Rev. Mod. Phys.*, **1969**, *41*, 48–81.
- (56) Feng, T.; Yao, W.; Wang, Z.; Shi, J.; Li, C.; Cao, B.; Ruan, X. Spectral Analysis of Nonequilibrium Molecular Dynamics: Spectral Phonon Temperature and Local Nonequilibrium in Thin Films and across Interfaces. *Phys. Rev. B*, 2017, 95, 195202.
- (57) Yalon, E.; Aslan, Ö. B.; Smithe, K. K. H.; McClellan, C. J.; Suryavanshi, S. V.; Xiong, F.; Sood, A.; Neumann, C. M.; Xu, X.; Goodson, K. E.; Heinz, T. F.; Pop, E. Temperature-Dependent Thermal Boundary Conductance of Monolayer MoS2 by Raman Thermometry. *ACS Appl. Mater. Interfaces*, **2017**, *9*, 43013–43020.
- (58) Hart, J. L.; Hantanasirisakul, K.; Lang, A. C.; Anasori, B.; Pinto, D.; Pivak, Y.; van Omme, J. T.; May, S. J.; Gogotsi, Y.; Taheri, M. L. Control of MXenes' Electronic Properties through Termination and Intercalation. *Nat. Commun.*, **2019**, *10*, 522.
- (59) Yasaei, P.; Behranginia, A.; Hemmat, Z.; El-Ghandour, A. I.; Foster, C. D.; Salehi-

- Khojin, A. Quantifying the Limits of Through-Plane Thermal Dissipation in 2D-Material-Based Systems. *2D Mater.*, **2017**, *4*, 035027.
- (60) Ma, T.; Liu, Z.; Wen, J.; Gao, Y.; Ren, X.; Chen, H.; Jin, C.; Ma, X.-L.; Xu, N.; Cheng, H.-M.; Ren, W. Tailoring the Thermal and Electrical Transport Properties of Graphene Films by Grain Size Engineering. *Nat. Commun.*, 2017, 8, 14486.
- (61) Zhao, W. L. Z.; Tikhonov, K. S.; Finkel'stein, A. M. Flexural Phonons in Supported Graphene: From Pinning to Localization. *Sci. Rep.*, **2018**, *8*, 16256.
- (62) Nika, D. L.; Pokatilov, E. P.; Askerov, A. S.; Balandin, A. A. Phonon Thermal Conduction in Graphene: Role of Umklapp and Edge Roughness Scattering. *Phys. Rev. B*, 2009, 79, 155413.
- (63) Colin-Ulloa, E.; Fitzgerald, A.; Montazeri, K.; Mann, J.; Natu, V.; Ngo, K.; Uzarski, J.; Barsoum, M. W.; Titova, L. V. Ultrafast Spectroscopy of Plasmons and Free Carriers in 2D MXenes. *Adv. Mater.*, **2022**, 2208659.
- (64) Tong, Z.; Li, S.; Ruan, X.; Bao, H. Comprehensive First-Principles Analysis of Phonon Thermal Conductivity and Electron-Phonon Coupling in Different Metals. *Phys. Rev. B*, 2019, 100, 144306.
- (65) Li, M.; Lu, J.; Luo, K.; Li, Y.; Chang, K.; Chen, K.; Zhou, J.; Rosen, J.; Hultman, L.; Eklund, P.; Persson, P. O. Å.; Du, S.; Chai, Z.; Huang, Z.; Huang, Q. Element Replacement Approach by Reaction with Lewis Acidic Molten Salts to Synthesize Nanolaminated MAX Phases and MXenes. J. Am. Chem. Soc., 2019, 141, 4730–4737.

Table of contents figure:

